IET Microwaves, Antennas & Propagation

*Research Article*

IET Journals
The Institution of Engineering and Technology

# Design of a uniplanar printed triple band-rejected ultra-wideband antenna using particle swarm optimisation and the firefly algorithm

ISSN 1751-8725
Received on 2nd November 2014
Revised on 16th June 2015
Accepted on 31st August 2015
doi: 10.1049/iet-map.2014.0736
www.ietdl.org

*Husham J. Mohammed[1,2], Abdulkareem S. Abdullah[1], Ramzy S. Ali[1], Raed A. Abd-Alhameed[2] ✉, Yasir I. Abdulraheem[1,2], James M. Noras[2]*

[1]*Department of Electrical Engineering, University of Basrah, Basrah, Iraq*
[2]*School of Engineering and Informatics, University of Bradford, Bradford, UK*
✉ *E-mail: r.a.a.abd@bradford.ac.uk*

**Abstract:** A compact planar monopole antenna is proposed for ultra-wideband applications. The antenna has a microstrip line feed and band-rejected characteristics and consists of a ring patch and a partial ground plane with a defective ground structure of rectangular shape. An annular strip is etched above the radiating element and two slots, one C-shaped and one arc-shaped, are embedded in the radiating patch. The proposed antenna has been optimised using bio-inspired algorithms such as the particle swarm optimisation and the firefly algorithm, based on a new software algorithm (Antenna Optimizer). Multi-objective optimisation achieves rejection bands at 3.3–3.7 GHz for Worldwide Interoperability for Microwave Access, 5.15–5.825 GHz for the 802.11a wireless local area network system or HIPERLAN/2, and 7.25–7.745 GHz for C-band satellite communication systems. Validated results show wideband performance from 2.7 to 10.6 GHz with $S_{11} < -10$ dB. The antenna has compact dimensions of $28 \times 30$ mm$^2$. The radiation pattern is comparatively stable across the operating band with a relatively stable gain except in the notched bands.

## 1 Introduction

Ultra-wideband (UWB) technology is increasingly important in applications such as sensor networks, medical imaging, multimedia communications, precision localisation systems, and ground-penetrating radar [1–6]. Due to its low complexity, ease of connection, and high data transmission rates, UWB has been used in many devices such as high definition TVs, laptops, wearable bio-medical sensors, and digital cameras. In such applications, the antenna is a critical component, required to be small enough to be integrated with other radio frequency circuits or embedded within wireless devices, with low cost, and stable radiation characteristics over a wide impedance bandwidth.

The 3.2–10.6 GHz frequency band for unlicensed UWB radio communication was released in February 2002 by the US Federal Communications Commission [7]. This band encompasses several existing narrow-band communication systems such as wireless local area network (WLAN) systems operating in the 5.15–5.825 GHz band, C-band satellite systems in the 7.25–7.745 GHz band, and Worldwide Interoperability for Microwave Access (WiMAX) operating in the 3.3–3.7 GHz band [8]; these narrow-band systems potentially can interfere with UWB systems. To suppress interference, it is possible to use a spatial filter [9]. Nevertheless, this method would increase the cost and complexity of the system, and would take up space when integrated with other microwave circuitry. Another way to filter out these narrow band systems from UWB applications is to design antennas with band-notch properties.

Various impedance matching principles are presented in the literature such as impedance matching optimisation through an embedded slot in the radiator [10–12]. In designing slots [13], the authors used the guided wavelength

$$\lambda_g = \frac{\lambda_{notch}}{\sqrt{\varepsilon_{eff}}} \quad (1)$$

$$\varepsilon_{eff} = \frac{\varepsilon_r + 1}{2} \quad (2)$$

where $\lambda_g$ and $\lambda_{notch}$ are the guided and notch wavelengths, respectively. $\varepsilon_r$ is the relative permittivity of the substrate.

Another technique proposed use parasitic patches to achieve a notched band [14]. Other examples include introducing an H-shaped slot close to the feeding point to filter out the WLAN band between 5.15 and 5.35 GHz [15], embedding complimentary split ring resonator (CSRR) slots and open-circuited stubs on the radiating elements to notch the WiMAX 3.3–3.7 GHz band and the WLAN 5.15–5.8 GHz band [16], inserting two elliptic single complementary split-ring resonators to filter out the WiMAX 3.3–3.8 GHz band and WLAN 5.15–5.85 GHz band [17], or placing two strips on the ground plane to reject the WLAN band operating at 5.15–5.85 GHz for portable UWB applications [18].

When considering global optimisation methods for antenna designs, bio-inspired algorithms such as genetic algorithms (GA) [19] and particle swarm optimisation (PSO) [20, 21], have been commonly used in the creation of design techniques that can satisfy constraints which would be otherwise unattainable.

This paper compares PSO with the firefly algorithm (FA), a population-based adaptive stochastic optimisation technique [22]. The application is the multi-objective optimisation of a uniplanar printed triple band-rejected UWB antenna. Current electromagnetic solvers do have some integrated optimisation tools that can aid antenna designers, but most of these tools do not allow designers to specify objective functions. With optimisation problems requiring difficult settings of objective functions, it would be desirable to express objective functions in a programming environment. The work reported here, the particular algorithms have been developed into novel software, used to design and optimise a simple and compact UWB.

## 2 Bio-inspired optimisation

### 2.1 Particle swarm optimisation

Like the GA, PSO is a population-based adaptive stochastic optimisation method, but differs in having no evolutionary factors

such as crossover, mutation, or selection: the method is based on the collective swarm intelligence observed in the social behaviour of birds, fish, bees and so on [23].

In PSO, the particles represent potential solutions to the optimisation problem, with an associated location and velocity; a fitness function is used to evaluate and compare locations. Each particle keeps track of its own best location, and the global location of the entire swarm. If a particle's current position has a better fitness value than its previous best location, the best location is updated by the current position: if any particle has a best position better than the current global position, that is also replaced.

In this paper, the application of the PSO is based on [20], where the update equations of velocity and position are given by

$$v_i^{k+1} = w^k v_i^k + c1 r_{1,i}^k \left(p_i^k - x_i^k\right) + c2 r_{2,i}^k \left(g_i^k - x_i^k\right) \quad (3)$$

$$x_i^{k+1} = x_i^k + \left(v_i^{k+1} \Delta t\right) \quad (4)$$

where $k$ refers to the current iteration, $i$ is the index of each particle, with $v_i^k$ and $x_i^k$ current velocities and positions, respectively. $w^k$ contains the inertial weights which set the effect of the particle's previous trajectory. $p_i^k$ gives each particle's best location, and $g_i^k$ is the global optimum. The parameters $c2$ and $c1$ are the social weight, and the cognitive weight, which determine whether a particle has a tendency towards the best position or towards the global position. More precisely, the cognitive parameter relates to the experience of each particle with respect to its best performance so far, while the social parameter relates to the best position found by either the whole swarm or a particle's neighbourhood. $r_{1,i}^k$ and $r_{2,i}^k$ are arbitrary numbers uniformly distributed in [0,1], and $\Delta t$ is the time step, normally set to unity.

### 2.2 Firefly optimisation

The FA was developed by Yang [22, 24], and is proposed for several different optimisation applications. It is a population-based adaptive stochastic optimisation method like PSO, inspired by the flashing patterns and characteristics of fireflies. The flashes are to attract

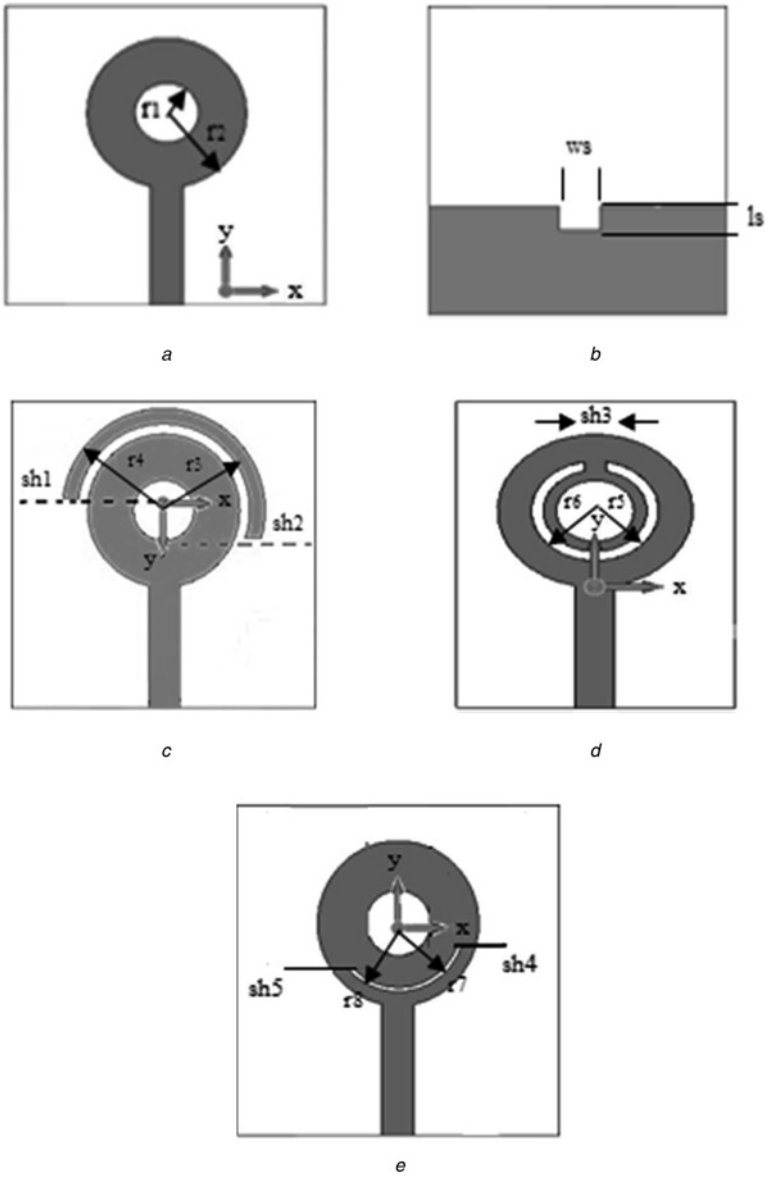


**Fig. 1** *Geometry of the*

*a* Primitive antenna (front view)
*b* Primitive antenna (bottom view)
*c* WLAN band-rejected antenna
*d* WiMAX band-rejected antenna
*e* C-band band-rejected antenna


*IET Microw. Antennas Propag.*, 2016, Vol. 10, Iss. 1, pp. 31–37

possible prey and to communicate or attract mating partners. Yang idealised some rules with respect to the real behaviour of fireflies:

(i) All fireflies are unisex: regardless of their sex, all fireflies are attracted to each other.
(ii) Attractiveness is proportional to brightness, brightness decreasing with increasing separation distance. A less bright firefly will move towards a brighter one; if there is no particularly bright attractor, movement is random.
(iii) The firefly's brightness is set by the cost function. In the simplest case, at a particular position $x$, the brightness $h(x)$ of a firefly is chosen as

$$h(x) = 1/f(x)$$

where $f(x)$ refers to the cost function.

The firefly's attractiveness $\beta$ depends on its brightness. Nevertheless, this attractiveness is relative, as judged by other fireflies. Therefore, it will be a function of the separation distance $r_{ij}$ between firefly $i$ and firefly $j$. The separation distance between any two fireflies $i$ and $j$ at $x_i$ and $x_j$, respectively, is the Cartesian distance $r_{ij}$ given by

$$r_{ij} = x_i - x_j = \sqrt{\sum_{k=1}^{p} (x_{i,n} - x_{j,n})^2} \quad (5)$$

where $x_{i,n}$ is the $n$th component of the spatial coordinate $x_i$ of firefly $i$, and $p$ is the dimension of each $x_i$ and $x_j$. With a fixed light absorption factor $\gamma$ for a given medium, $\beta$ varies with $r_{ij}$

$$\beta(r) = \beta_0 e^{-\gamma r_{ij}^2} \quad (6)$$

where $\beta_0$ is the attractiveness at $r_{ij} = 0$.

Firefly $i$ is moved by attraction to another firefly $j$ that should be more bright, attractive or repulsed by firefly $j$ that has less bright. This movement is given by

$$x_i^{m+1} = x_i^m + \beta_0 e^{-\gamma r_{ij}^2}\left(x_j - x_i^m\right) + \alpha\left(\text{rand} - \frac{1}{2}\right) \quad (7)$$

where $m$ refers to the current iteration and $x_i$ is the current position. The second term gives the effect of attraction whereas the third term expresses the randomisation: $\alpha$ is the randomisation factor, $\alpha \in [0, 1]$. rand is an arbitrary number uniformly distributed in [0, 1].

## 3 Single band-rejected antennas design

### 3.1 Primitive antenna

Figs. 1*a* and *b* show the geometry of the primitive annular patch antenna, which is printed on one side of an FR4 substrate with a relative dielectric constant of 4.4, thickness 1.6 mm, and dimensions $30 \times 30$ mm$^2$. The radiation element is the annular patch that is fed by a microstrip line of width 3 mm and length 12 mm. The inner $r_1$ and outer $r_2$ radius values are 3 and 8 mm, respectively. A partial ground is printed on the other side of the substrate with a width of 30 mm and length 12 mm. A defective ground structure is used as a rectangular shaped with dimensions of $ws \times ls$ mm$^2$, where $ws$ and $ls$ are equal to 2 and 1 mm, respectively.

### 3.2 Antenna with parasitic annular strip

WLAN radio signals already occupy specific frequencies in the UWB band, between 5.15 and 5.825 GHz, and so might interfere with UWB systems unless band-rejection was introduced.

Fig. 1*c* shows the antenna geometry. A semi-circular annular strip with an inner radius $r_3$ of 8.5 mm and an outer radius $r_4$ of 9.7 mm has been etched above the annular patch, resulting in high impedance at the particular notch frequency. The length of this strip is bounded by two plane edges, sh1 and sh2. The effective length of the annular strip is 33.2 mm which should equal the guided wavelength for the required notch frequency of 5.5 GHz, as calculated by (1). Thus, the corresponding values of sh1 and sh2 will be approximately 1 and 5.3 mm, respectively.

### 3.3 Antenna with a C-shaped slot

WiMAX operates in the range of 3.3–3.7 GHz and so might interfere with UWB devices. A C-shaped slot is cut in the primitive antenna as shown in Fig. 1*d*, intended to minimise potential interference. The values of the inner radius $r_5$ and outer radius $r_6$ are 4 and 4.5 mm, respectively. The length of the slot is bounded by the plane edge sh3. The effective length of the C-shaped slot should be around half the guided wavelength at the required notch frequency of 3.45 GHz, calculated using (1) as 26.5 mm. Therefore, sh3 will be approximately 3 mm.

### 3.4 Antenna with an arc-shaped slot

C-band satellite systems operate at 7.25–7.745 GHz, another potential source of interference, requiring a band-notched characteristic at these frequencies. Fig. 1*e* shows the geometry of the modified antenna. An arc-slot with an inner radius $r_7$ and an outer radius $r_8$ of 5.9 and 6.4 mm, respectively, has been embedded in the radiating element, which leads to high impedance at the notch frequency. The length of this strip is bounded by two plane edges sh4 and sh5. The effective length of the arc-slot should be around half the guided wavelength of the required notch frequency 7.4 GHz given by (1), calculated as 12.3 mm. Therefore, the values of sh4 and sh5 will be approximately 2 and 4 mm, respectively, but in the negative direction of the $y$-axis.

The simulated input reflection coefficients of the primitive and single band-notch antennas are shown in Fig. 2.

## 4 Parameters study

To investigate the key parameters, the antenna with the parasitic annular strip is now analysed as an example.

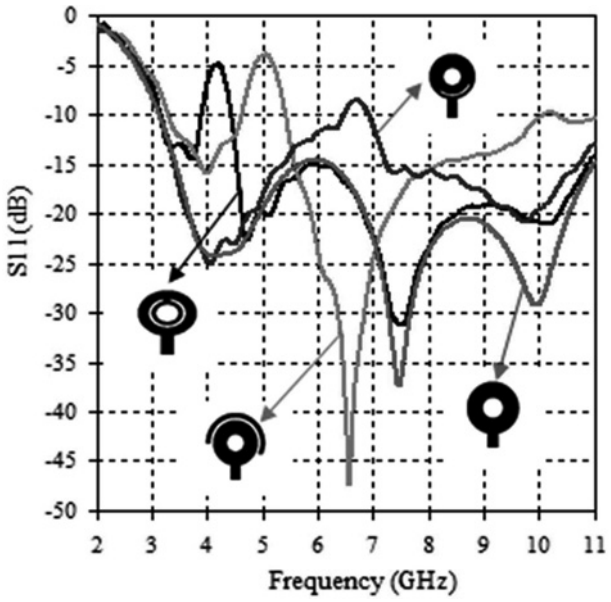


**Fig. 2** *Simulated input reflection coefficients*

Fig. 3 shows the reflection coefficient curves of the antenna for various values of sh1, keeping sh2 at 1 mm. It is noticed that as sh1 increases from 2 to 6 mm, the centre frequency of the notch band decreases from 5.78 to 5.08 GHz.

Fig. 4 illustrates the reflection coefficient curves with sh1 = 0, for sh2 varying from 2 to 6 mm, where the centre frequency of the notch band varies from 6 to 5.2 GHz. Later, Fig. 5 illustrates the reflection coefficient curves with $r_3 = 8.5$ mm for $r_4$ varying from 8.8 to 9.6 mm, where the notched bandwidth increased. The effect of sh1 has the same type of effect as sh2 because both are related to the length of the parasitic element. From the above parametric study, it can be concluded that the centre frequency of the notch band can be controlled by varying the values of sh1 and sh2. The width of the notch band can be controlled by changing the width of the parasitic element.

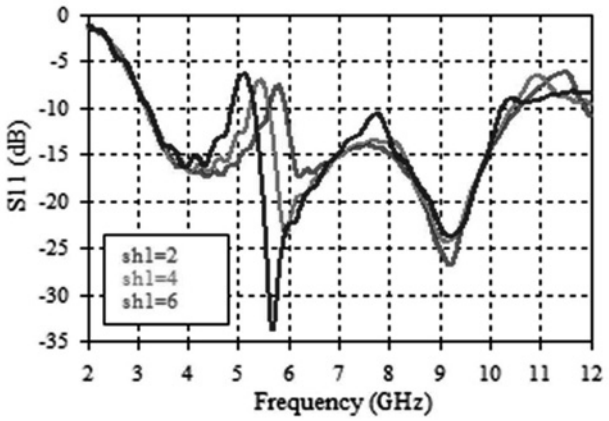


**Fig. 3** *Reflection coefficients for different values of sh1*

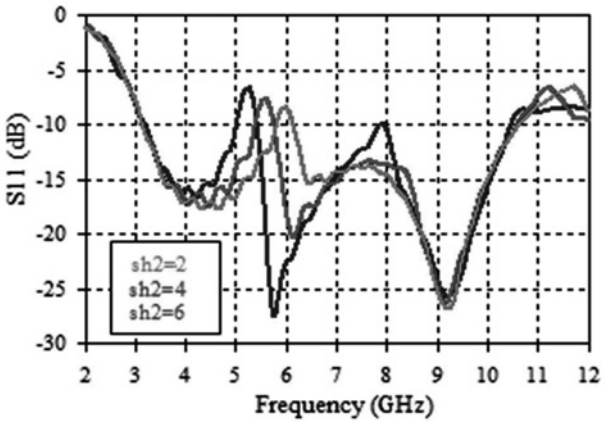


**Fig. 4** *Reflection coefficient for different values of sh2*

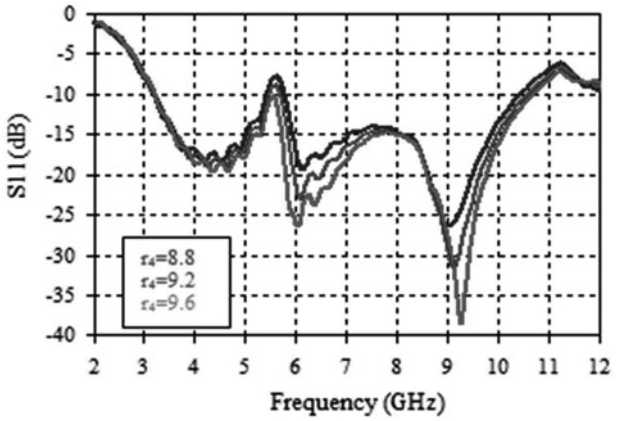


**Fig. 5** *Reflection coefficient for different values of $r_4$*

## 5 Triple band-rejected antenna design

### 5.1 Antenna geometry

Fig. 6 shows the composite geometry of the triple band-notch UWB antenna which is the combination of the previous three structures. Comparing with Fig. 2 it can be seen that the resulting notch band of each antenna can be above or below that of the individual cases, and the values of $S_{11}$ in the notched bands is not enough to prevent interference with the narrow band system. So, the notching frequencies need to be tuned, and their return loss values improved: these targets can be expressed as objective functions for the bio-inspired optimisation.

### 5.2 Objective functions

Two objectives are to be satisfied. Each objective with its corresponding cost function is described below, and then the separate cost functions are combined into a single fitness function

$$\mathrm{Gf1} = \sum_{f_1}^{f_2} p(f) + \sum_{f_3}^{f_4} p(f) + \sum_{f_5}^{f_6} p(f) \tag{8}$$

$$\text{where } p(f) = \begin{cases} 0 & \text{for } S_{11} \geq -4 \\ -S_{11} & \text{for } S_{11} < -4 \end{cases}$$

$$\mathrm{Gf2} = \sum_{f_2+0.01}^{f_3-0.01} k(f) + \sum_{f_4+0.01}^{f_5-0.01} k(f) + \sum_{f_6+0.01}^{f_7} k(f) \tag{9}$$

$$\text{where } k(f) = \begin{cases} -S_{11} & \text{for } S_{11} \geq -10 \\ 0 & \text{for } S_{11} < -10 \end{cases}$$

$$\mathrm{Gf} = \left| \frac{1}{(\mathrm{Gf1} + \mathrm{Gf2}) + 1} - 1 \right| \tag{10}$$

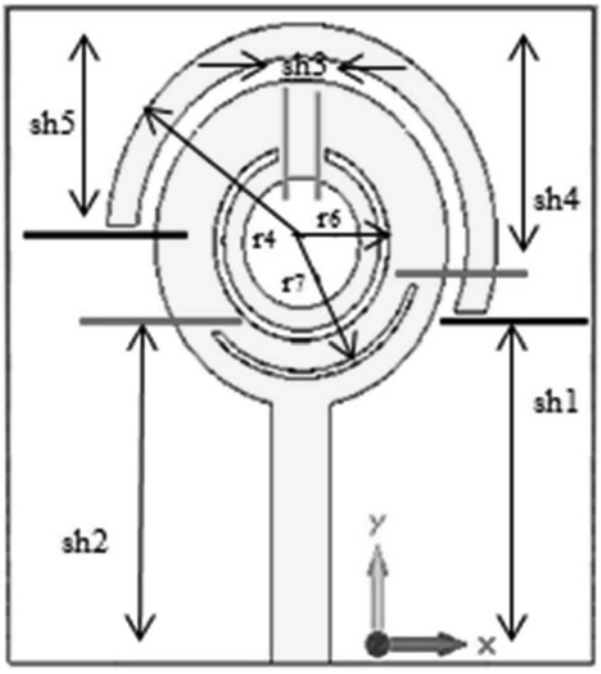


**Fig. 6** *Geometry of the triple band-notch antenna*


*IET Microw. Antennas Propag.*, 2016, Vol. 10, Iss. 1, pp. 31–37

where $S_{11}$ is the input reflection coefficient loss in dB, $f_1$ and $f_2$ are the lower and upper frequencies for the WiMAX band, respectively, $f_3$ and $f_4$ are the lower and upper frequencies for the WLAN band, respectively, $f_5$ and $f_6$ are the lower and upper frequencies for the C-band satellite communication systems, respectively, and $f_7$ is the highest frequency of the UWB band. $N$ is the number of frequency samples taken between $f_1$ and $f_7$. Gf1 is the cost function responsible for a band's rejection whereas Gf2 is the cost function responsible for making the reflection coefficient in the other bands less than –10 dB. Gf is the overall fitness function. We can conclude from the conditions of (8) and (9) that the best possible fitness value is 0. However, if any other antenna parameters (e.g. peak gain or specific radiation pattern in the plane) are described well and merged into the specific overall fitness function given in (10), subject to appropriate weightings, then it is possible to improve or modify that parameter or parameters. The present work has not considered such an extended optimisation procedure.

### 5.3 Antenna optimiser software

For the optimisation, an interface between MATLAB [25] and the electromagnetic simulator CST Microwave Studio [26], called 'Antenna Optimizer', has been created, based on the graphical user interface tools of MATLAB. This enables MATLAB to control the optimisation in an automated design process, as shown in Fig. 7.

## 6 Simulated and measured results

The parameter study identified some of the key antenna parameters for the notching characteristics, to be used in optimisation with the PSO and the FA. The parameters' domain limits are given in Table 1, and the other parameters needed by the particular algorithms are given in Table 2. The population size, number of variables, variable limits, and the number of iterations are the same for the PSO and the FA.

**Table 1** Values of antenna parameter limits

| Parameters | Min_Values, mm | Max_Values, mm |
|---|---|---|
| sh1 | –2 | 2 |
| sh2 | 0 | 5 |
| sh3 | 0 | 4 |
| sh4 | –6 | 0 |
| sh5 | –5 | 0 |
| $r_4$ | 8.8 | 10 |
| $r_6$ | 4.5 | 5.3 |
| $r_8$ | 6 | 7 |
| *ws* | 1 | 6 |
| *ls* | 1 | 5 |

**Table 2** Algorithms parameter values

| Algorithm | Parameter | Value |
|---|---|---|
| PSO | population size | 20 |
| | *N* variables | 10 |
| | *N* iterations | 20 |
| | *c*1 | 2 |
| | *c*2 | 2 |
| | *w* | 0.65 |
| | steps = population size * *N* iterations | 400 |
| FA | $\gamma$ | 1 |
| | $\alpha$ | 0.5 |
| | $\beta$ | 0.2 |

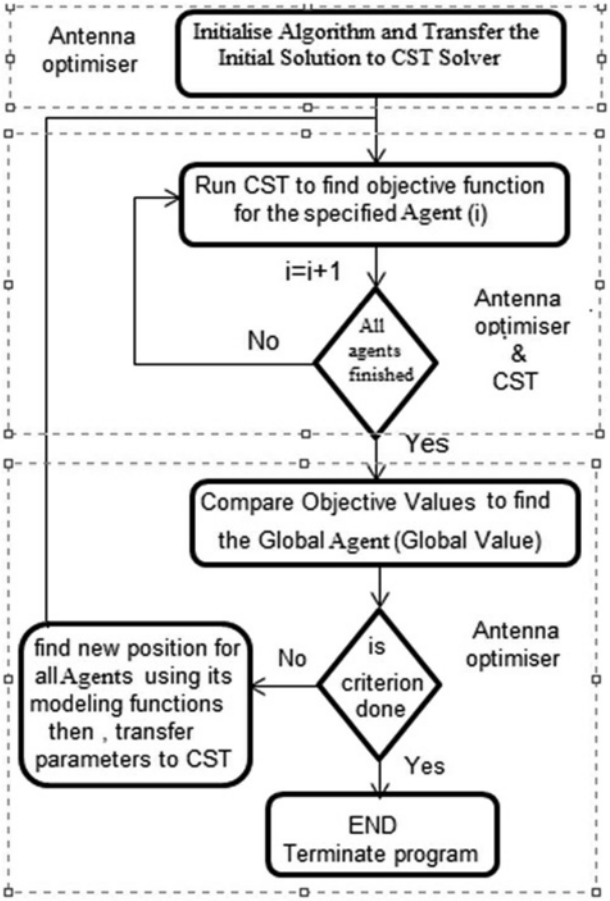


**Fig. 7** *Automated design process*

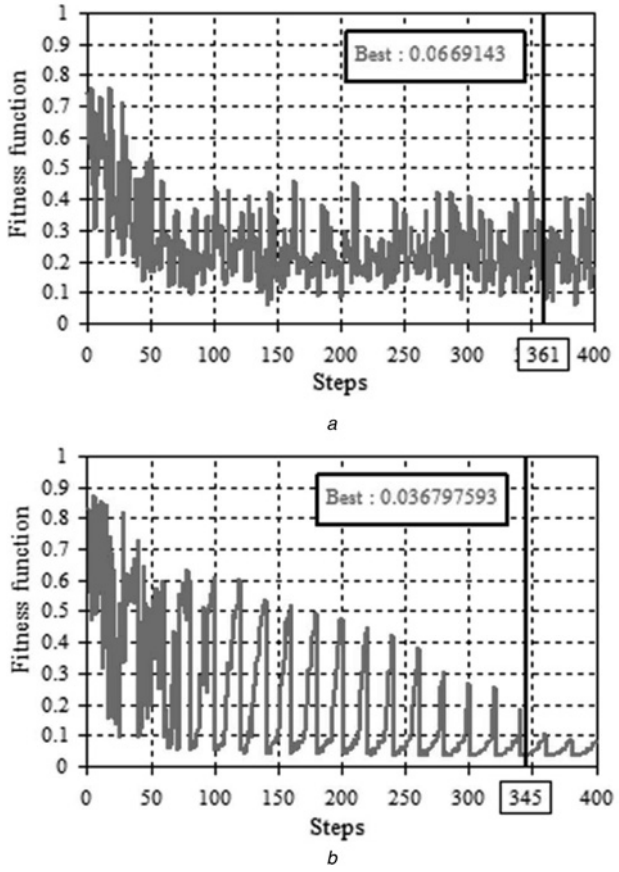


**Fig. 8** *Fitness functions of*
*a* PSO
*b* FA

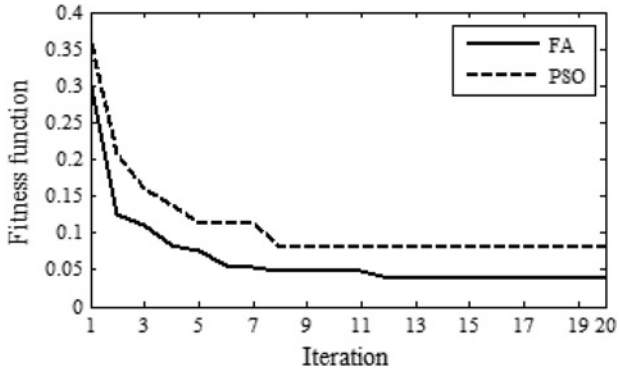


**Fig. 9** *Optimal agents fitness values for the PSO and the FA*

**Table 3** Optimal values of antenna parameters

| Parameters | Optimal values, mm |
|---|---|
| sh1 | 0.248459 |
| sh2 | 3.661857 |
| sh3 | 2.492596 |
| sh4 | −4.858249 |
| sh5 | −1.656952 |
| $r_4$ | 9.898860 |
| $r_6$ | 4.906965 |
| $r_8$ | 6.623525 |
| *ws* | 3.569930 |
| *ls* | 2.993580 |

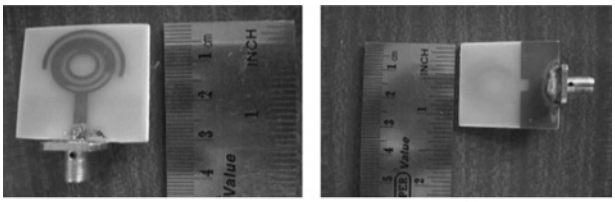


**Fig. 10** *Fabricated antenna*

*a* Front view
*b* Rear view

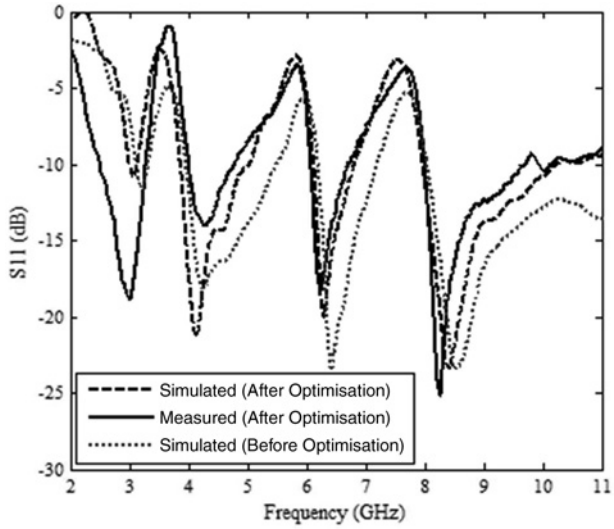


**Fig. 11** *Simulated and measured reflection coefficients*

Running on an HP Compaq 8200 Elite CMT PC with 16 GB RAM and 3.4 GHz CPU, a single fitness function evaluation took some 7–10 min and an entire algorithm optimisation run took 3–4 h. The fitness functions of the particular algorithms are shown in Fig. 8. The FA optimised design reached a fitness value of 0.036 at step 345, whereas for the PSO the fitness value was 0.066 at step 361.

Fig. 8 gives a clear view of the behaviour of the agents throughout the search domain, whereas Fig. 9 shows the best agent fitness values in each iteration of the specific algorithms.

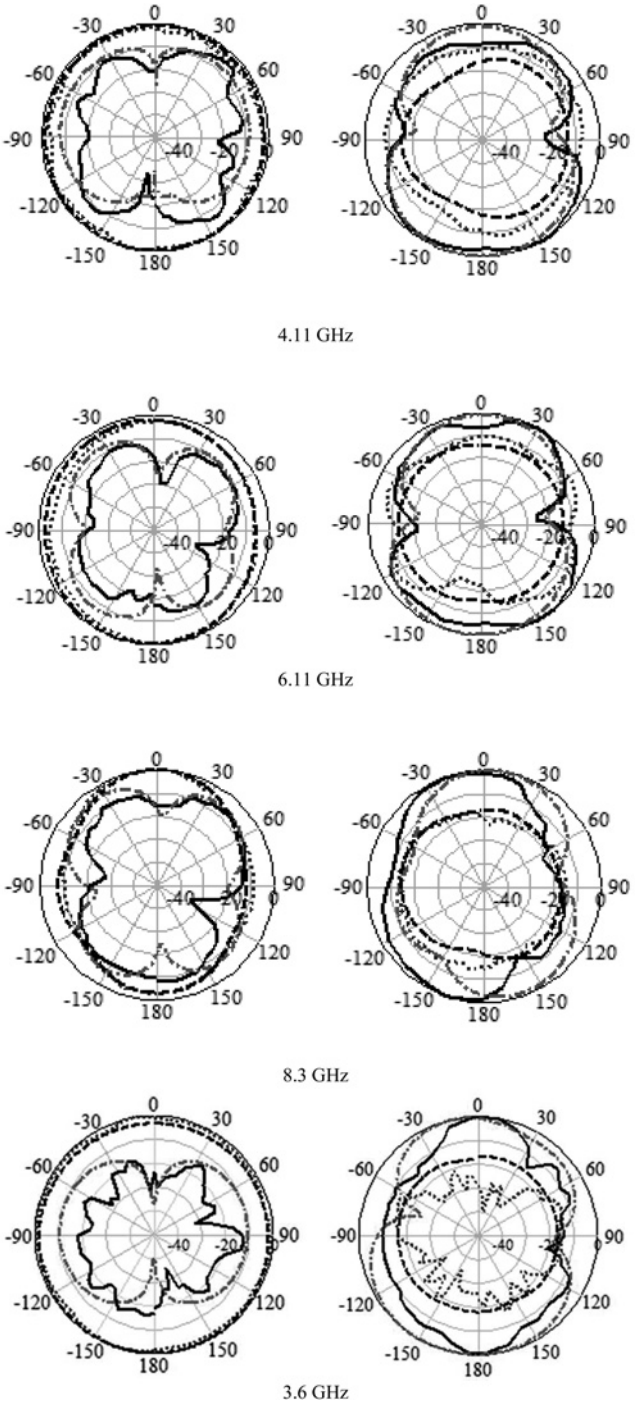


**Fig. 12** *Simulated and measured radiation patterns*

*a* In *xz*- plane and
*b* In *yz*- plane
Simulated $E_\Theta$: dashed-dotted line. Measured $E_\Theta$: solid line. Simulated $E_\varphi$: dashed line. Measured $E_\varphi$: dotted line

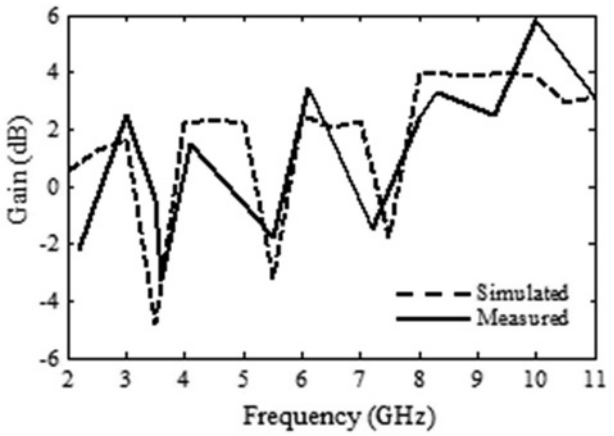


**Fig. 13** *Simulated and measured realised gain versus frequency*

From Figs. 8 and 9, it can be seen that the FA is faster than the PSO and achieved better fitness values. The behaviour of FA agents' fitness values is more stable than with PSO: fireflies worked almost individually and grouped more closely around each optimal point without hopping around as in PSO.

Based on the FA optimal parameters shown in Table 3, the antenna was fabricated and is shown in Fig. 10. $S_{11}$ was measured using the HP 8510C Network Analyzer. Fig. 11 displays the measured and simulated $S_{11}$ results of the designed antenna, showing a wideband performance from 2.7 to 10.6 GHz for $S_{11} < -10$ dB.

The normalised simulated and measured radiation patterns in the *xz* and *yz* planes at 4.11, 6.11, 8.3, and 3.6 GHz are shown in Fig. 12. $E_{\varphi}$ represents the co-polarisation properties, and $E_{\Theta}$ represents the cross-polarisation properties. The cross-polarisation dimensions are smaller than the co-polarisation dimension in the *xz*-plane at the resonances 4.1, 6.11, 8.3, and 3.6 GHz, whereas the co-polarisation dimensions are smaller than the cross-polarisation dimension in the *yz*-plane. The antenna has nearly omnidirectional radiation patterns.

The measured and simulated gains from 2 to 11 GHz, see Fig. 13, show that the gain decreases sharply around 3.55, 5.5, and 7.2 GHz. Outside the notch band gains varying less than 5.8 dB are achieved, indicating stable performance across the operating bands.

## 7 Conclusions

This study presents a compact, simple microstrip-fed printed monopole UWB antenna with triple band-rejected facility. To obviate possible interference between UWB systems and narrowband WLAN, WiMAX, and C-band satellite communication systems, an annular patch as a parasitic element, a C-shaped slot and an arc-slot are added for band rejection. Positioning of the desired rejected bands was achieved by optimising the antenna parameters using the PSO and the FA based on novel software (Antenna Optimizer Software). The FA, which has not been applied to this type of problem before, gives a better result than the PSO.

Both simulations and measurements show that the antenna has triple notched bands over an ultra-wide operation band, combined with a good radiation pattern and useful gain. The compact size, simple structure, and excellent performance of the antenna make it a good candidate for various UWB applications.

## 8 Acknowledgments

This work was supported in part by the United Kingdom Engineering and Physical Science Research Council (EPSRC) under Grant EP/E022936A, TSB UK under grant application KTP008734 and the Iraqi Ministry of Higher Education and Scientific Research.

## 9 References

1 Bialkowski, M.E., Khor, W.C., Crozier, S.: 'A planar microwave imaging system with step-frequency synthesized pulse using different calibration methods', *Microw. Opt. Technol. Lett.*, 2006, **48**, pp. 511–516
2 Turk, A.S., Nazli, H.: 'Hyper-wide band TEM horn array design for multi band impulse ground penetrating radar', *Microw. Opt. Technol. Lett.*, 2008, **50**, pp. 76–81
3 Viani, F., Lizzi, L., Azaro, R., *et al.*: 'A miniaturized UWB antenna for wireless dongle devices', *IEEE Antennas Wirel. Propag. Lett.*, 2008, **7**, pp. 714–717
4 Islam, M.T., Misran, N., Mobashsher, A.T.: 'Compact dual band microstrip antenna for ku-band application', *Inf. Technol. J.*, 2009, **9**, pp. 354–358
5 Mei, H.D., Yu, Z.Q.: 'Impulse radio ultra-wide-band through wall imaging radar based on multiple-input multiple-output antenna arrays', *Inf. Technol. J.*, 2010, **9**, pp. 782–789
6 Islam, M.T., Azim, R., Misran, N.: 'Linear polarized patch antenna for satellite communication', *Inf. Technol. J.*, 2010, **9**, pp. 386–390
7 Federal Communications Commission, Washington, DC, 'FCC report and order on ultra-wideband technology', 2002
8 Lin, C.C., Jin, P., Ziolkowski, R.W.: 'Single, dual and tri-band-notched ultra-wideband antennas using capacitively loaded loop resonators', *IEEE Trans. Antennas Propag.*, 2012, **60**, (1), pp. 102–109
9 Yeo, J., Mittra, R.: 'A novel wideband antenna package design with a compact spatial notch filter for wireless applications', *Microw. Opt. Technol. Lett.*, 2002, **35**, pp. 455–460
10 Xu, P., Yan, Z., Zhang, T., *et al.*: 'Broadband circularly polarized slot antenna array with fan-shaped feed line and L-shaped grounded strips', *Prog. Electromagn. Res. Lett.*, 2014, **44**, pp. 125–131
11 Tang, M.-C., Ziolkowski, R.W.: 'Compact hyper-band printed slot antenna design and experiments'. The 8th European Conf. on Antennas and Propagation (EuCAP), 2014, pp. 594–596
12 Sahu, B., Jain, P.: 'Dual band antenna design with improved result for mobile and satellite application', *Int. J. Electron. Commun. Eng.*, 2014, **1**, (7), pp. 50–55
13 Nguyen, T.D., Lee, D.H., Park, H.C.: 'Design and analysis of compact printed triple band-notched UWB antenna', *IEEE Antennas Wirel. Propag. Lett.*, 2011, **10**, pp. 403–406
14 Kim, K.H., Cho, Y.J., Hwang, S.H., *et al.*: 'Band-notched UWB planar monopole antenna with two parasitic patches', *Electron. Lett.*, 2005, **41**, pp. 783–785
15 Ur-Rehman, M., Abbasi, Q.H., Akram, M., *et al.*: 'Design of band-notched ultra wideband antenna for indoor and wearable wireless communications', *IET Microw. Antennas Propag.*, 2015, **9**, (3), pp. 243–251
16 Huang, H., Liu, Y., Gong, S.: 'Uniplanar differentially driven UWB polarization diversity antenna with band-notched characteristics', *Electron. Lett.*, 2015, **51**, (3), pp. 206–207
17 Sarkar, D., Srivastava, K.V., Saurav, K.: 'A compact microstrip-fed triple band-notched UWB monopole antenna', *IEEE Antennas Wirel. Propag. Lett.*, 2014, **13**, pp. 396–399
18 Liu, L., Cheung, S.W., Yuk, T.I.: 'Compact MIMO antenna for portable UWB applications with band-notched characteristic', *IEEE Trans. Antennas Propag.*, 2015, **63**, (5), pp. 1917–1924
19 Haupt, R.L., Werner, D.H.: 'Genetic algorithms in electromagnetics' (IEEE Press Wiley-Interscience, 2007)
20 Robinson, J., Rahmat-Samii, Y.: 'Particle swarm optimization in electromagnetics', *IEEE Trans. Antennas Propag.*, 2004, **52**, (2), pp. 397–407
21 Liu, W.C.: 'Design of a multiband CPW-fed monopole antenna using a particle swarm optimization approach', *IEEE Trans. Antennas Propag.*, 2005, **53**, (10), pp. 3273–3279
22 Yang, X.S.: 'Multi-objective firefly algorithm for continuous optimization', *Eng. Comput.*, 2013, **29**, (2), pp. 175–184
23 Eberhart and Kennedy: 'Particle swarm optimization'. IEEE Int. Conf. on Neural Networks, 1995
24 Yang, X.S.: 'Firefly algorithms for multimodal optimization'. Proc. 5th Int. Conf. on Stochastic Algorithms: Foundations and Applications, SAGA 2009, 2009 (LNCS, 5792), pp. 69–178
25 MATLAB: Mathematics Lab: 'The language of technical computing' (Mathworks, 2013), Ver.7.8.0.347
26 'CST: Computer Simulation Technology Based on FIT Method', CST Computer Simulation Technology, 2014